

Snake robot traversing large obstacles using vertical bending with force feedback

Qiyuan Fu and Chen Li

Abstract— Snake robots hold the promise as a versatile platform to traverse complex environments. Previous snake robots often used lateral bending to push against vertical structures on flat surfaces. Recent animal experiments revealed that vertical bending is also important for generating propulsion during traversal of terrain with large height variation. Although snake robots can propagate a vertical bending shape to passively push to traverse such terrain, it is possible that active pushing modulated by contact force and internal torque sensing can further help control propulsion. Here, we explore this question by testing a previously developed robot with contact forces sensors added. We tested the robot using vertical bending to traverse a large obstacle and compared five controllers without and with various sensory feedback using various force and torque information, as well as various load and terrain conditions to perturb the system. Feedforward propagation of vertical bending that conforms to the terrain *a priori* can produce propulsion but fails with terrain perturbation that breaks conformation. In general, sensory feedback helps better maintain or regain contact and propulsion, but different types of feedback displayed different tradeoffs and varied performance. We also identified issues that needs improvement in further development.

Index Terms—Locomotion, snakes, sensory feedback, gait, propulsion.

I. INTRODUCTION

With their slender and highly flexible body, snake robots hold the promise as a versatile platform to traverse a diversity of environments [1], especially complex terrain with large obstacles [2]–[5] that challenge wheeled and legged robots. Similar to snakes [4], [6], [7], several snake robots have been developed to use lateral bending to push against vertical structures to move on flat surfaces [8]–[13]. However, beyond such surfaces, snakes often traverse 3-D terrain with large height variation, such as large boulders and fallen trees [5], [14], [15]. Several snake robots can accommodate height variations using gaits designed for flat surfaces with controlled compliance [16]–[18]. A few others use complex geometric path or shape planning for dedicated environments such as pipelines and steps [19]–[21]. Still, beyond simply using vertical bending to connect multiple functional segments, we have rarely considered whether and how vertical bending can contribute to propulsion.

DATE OF SUBMISSION, ETC. This work was supported by a Burroughs Wellcome Fund Career Award at the Scientific Interface, an Arnold and Mabel Beckman Foundation Beckman Young Investigator Award, and The Johns Hopkins University Whiting School of Engineering start-up funds.

Recent animal studies revealed that snakes can use vertical bending to push against terrain of significant height variation to traverse, such as a horizontal ladder (Fig. 1A), a wedge (Fig. 1B) [15], or uneven rubble-like terrain [22]. The snakes seemingly simply propagate a vertical bending shape down the body to achieve this. However, it is likely that this process is sensory-modulated. Snakes have both mechanoreceptors (tactile sensing) within the skin and proprioceptors (internal position, motion, and force sensing) within the muscles and tendons [23]–[25]. Generalist snakes moving on flat surfaces with vertical structures have been found to adjust lateral body bending to maintain contact with and modulate propulsion generated against vertical structures [6], [7], presumably using these senses for feedback control.

Two snake robots used feedforward vertical bending propagation after the head to passively push against terrain with height variation to traverse [8], [15]. However, it is possible that active pushing modulated by contact force and internal torque sensing feedback may further help snake robots control propulsion during traversal. Here, to begin to understand this, we study how well a snake robot traverses a large obstacle using vertical bending with different types of contact force and/or internal torque feedback control. We hypothesize that the robot will traverse by feedforward propagation of a bending shape that matches obstacle geometry [15], [19], but it will struggle in novel terrain of different shapes. We hypothesize that using contact force and internal torque feedback can help conform to and push against the environment to generate propulsion.

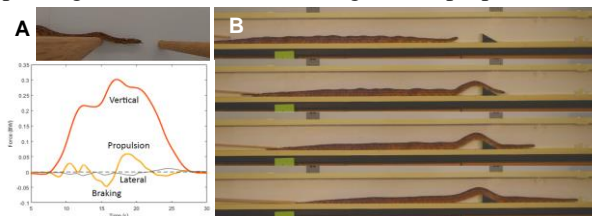


Fig. 1. Animal observations (A) Vertical (red), fore-aft (orange), and lateral (gray solid) forces during a vertical undulation on a horizontal ladder. (B) Side view of a snake traversing a wedge using vertical bending. The snake transitions from a concertina gait to using vertical bending only once it has sufficient contact with the wedge. Reproduced from [15].

We equipped a recently developed snake robot [26] with force sensors as a test platform (Section II). To generate vertical bending and study whether and what types of force feedback help robots better traverse obstacles while conforming to terrain variations, we used five controllers with different types of contact force or internal torque feedback control (Section III):

The authors are with the Department of Mechanical Engineering, Johns Hopkins University, Baltimore, MD 21218 USA (e-mail: fqiyan1@jhu.edu; chen.li@jhu.edu). Corresponding author: Chen Li

(A) pure shape propagation with no contact force feedback, (B) shape propagation with head conforming to terrain shapes using only contact force feedback at the head, (C) shape propagation with body partially conforming to terrain shapes using whole body contact force feedback, (D) shape propagation with active pushing against terrain using whole body contact force feedback and internal torque feedback [13], and (E) internal torque-based shape propagation with head conforming to terrain shapes with no contact force feedback [8]. For each controller, we challenged the robot to traverse a large obstacle in five different cases (Section IV) with: (a) no backward load, (b) small backward load, (c) large backward load, (d) another obstacle in the front, and (e) poor initial terrain conformation. (a-c) are designed to test how well different controllers generate propulsion, (d) is to test their abilities to conform to new terrain contacts, and (e) is to test their abilities to handle changes in existing contacts. We tracked the positions of robot body, recorded force data, and evaluated the performance by comparing lift-off height and propulsion generated by pushing against the large obstacle (Section V). Finally, we summarize the findings in our experiments and discuss future work (Section VI).

II. ROBOT STRUCTURE

We used a recently developed snake robot [21] (1.07 m long, 2.254 kg) with 9 pitch and 9 yaw joints alternating. The alternating joint structure is common for snake robots capable of 3-D motions [17], [19], [20], [27], [28]. Because we only study vertical bending, the yaw joints were fixed to be straight. All joints are actuated by Dynamixel XM430-W350R servo motors. A pair of passive wheels were installed at the anterior end of each link to reduce friction (friction coefficient $\mu = 0.06$) [21]. Because there is no lateral bending or movement present in this study, the friction anisotropy, including the one-way mechanism [21], [29] is not used for propulsion. Each wheel was installed on an arm that can freely rotate around a shaft fixed to the link (Fig. 2B). A compression spring is added between each wheel and link for additional mechanical compliance to improve contact and absorb collisional impact.

To measure ground reaction forces, we installed a force sensing resistor [28] (FSR-400 short) between each wheel and the corresponding spring (Fig. 2B). To fixate and protect the sensor, we installed it on a separate arm (Fig. 2B, blue) that rotates freely around the shaft of the wheel arm (Fig. 2B, orange). In its small range of arm rotation (10°), the FSR surface stays nearly parallel to the link it is installed to. Four Sparkfun ADS-1015 ADC breakouts and an Arduino Mega 2560 board were used to collect the voltage output of 20 sensors and send the results to a desktop computer at a sampling frequency of 62 Hz. Controllers were implemented in Robotic Operating System and ran at 100 Hz.

All force sensors were calibrated on-site before the experiments. Calibration was performed by pulling the shaft of each wheel upward with a variable weight w via a pulley system while recording corresponding output voltage of the circuit V . The robot was fixed to be straight and horizontal during calibration. The resistance of each force sensor R was then calculated from the voltage. A linear interpolation $\log w =$

$k_{FSR} \log R + b_{FSR}$ was used for real-time contact force feedback and data analysis, where k_{FSR} and b_{FSR} were fitted from calibration data (Fig. 3). During experiments, the robot estimated each force F_i to be normal to link i .

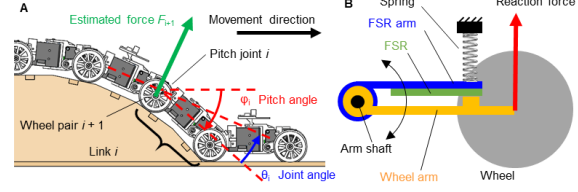


Fig. 2. Design of the robot. (A) Overall structure. Each pitch joint i connects rigid link i and $i+1$, and sits right above $i+1$ -th pair of wheels. Green vector shows direction of estimated force acting on wheel pair $i+1$. (B) Wheel and FSR installation. Wheel (gray) has its shaft attached to wheel arm (yellow), which has an extruded pad to push on FSR (green). FSR is fixated to FSR arm (blue) that compresses a spring when being pushed upward. Both arms rotate around arm shaft (black) independently.

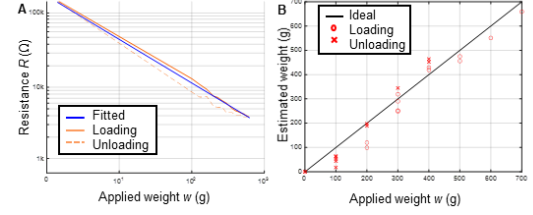


Fig. 3. Force sensing resistor calibration. (A) Measured resistance as a function of applied weight during loading (orange solid) and unloading (orange dash). Blue line is the linear fit. (B) Estimated weight using calibrated model as a function of applied force for loading (circle) and unloading (cross).

III. CONTROLLER DESIGN

We implemented five different controllers to propagate a vertical shape down the body with different additional functions. Controllers A-D below control joint angles directly, whereas controller E controls joint torque. To maintain stability of test results and accommodate a feedback frequency of 62 Hz and potentially high latency, propagation speed and gains in the controllers were set to be small.

A. Pure shape propagation

This controller propagates an arbitrary bending shape down the body using a follow-the-leader strategy that linearly shifts each joint angle toward that of the joint anterior to it:

$$\theta_i(t) = \theta_{i-1}(nT) \cdot \frac{t-nT}{T} + \theta_i(nT) \cdot \frac{(n+1)T-t}{T}, nT \leq t < (n+1)T, i \geq 2 \quad (1)$$

where t is the current time, T is the time taken to shift one joint angle down one link (hereafter referred to as the period), n is the number of periods that have passed, i is the index of the joint counting from the head. After each period, the shape will be shifted down the body by one link length.

As the initial shape is propagated down the body, new curve shapes will be determined by the motion of the head. In this controller, the first pitch joint is controlled with a pre-determined profile to linearly decay to 0 (straight) and become straight after one period:

$$\theta_1(t) = \begin{cases} \theta_1(0) \cdot \frac{t}{T}, & t < T \\ 0, & t \geq T \end{cases} \quad (2)$$

With this controller, the initial shape was only propagated down the body once before the robot became completely

straight. A typical trial using pure shape propagation is shown in Fig. 4.

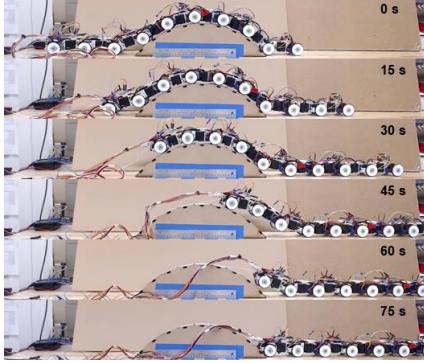


Fig. 4. Representative webcam snapshots of robot traversing a large obstacle using pure propagation.

B. Shape propagation with head conforming to terrain

The second controller allows the head to conform to new terrain encountered and propagates this new shape down the body. It controls the pitch joint 1 to maintain a constant contact force on the wheel pair 1 instead of using the pre-determined profile:

$$\dot{\theta}_1(t) = k_1(F_1 - \bar{F}) \quad (3)$$

where k_1 is a constant gain, F_1 is the sum of forces detected on the first pair of wheels, and \bar{F} is the desired contact force.

For the rest of the pitch joints, this controller uses the same follow-the-leader strategy as Eqn. (1).

C. Shape propagation with partial conformation to terrain

This controller controls the robot to maintain contact with the front side of terrain surfaces and propagate this shape down the body. To do so, it performs a two-step operation in each control cycle: first, it propagates a shape using Eqn. (1); second, it conforms parts of the body that are above the front side of terrain surfaces to conform to the terrain using contact force feedback. The sum of the change of angles from these two steps are then sent to servo motors as the goal positions of this cycle.

Conforming is triggered on joint i and its adjacent joints $i-1$ and $i+1$ if both of the following conditions are satisfied: (a) Force F_i is smaller than 0.5 N (25% of the weight of one link). This indicates that wheel pair i might have lost contact considering force feedback noises. (b) Pitch angle of the $(i+1)$ -th link ϕ_{i+1} (Fig. 2A) is non-positive, which indicates that it is not likely to push against the back side of terrain surfaces if conforming is applied. This asymmetric triggering condition prevents links from pushing on the back side of the obstacle which could generate large forward resistance.

To estimate pitch angles with no external pose feedback, we assumed that the line segment connecting the head and the tail remained horizontal considering that the height difference of the head and the tail in these tests were usually small. We then calculated pitch angles of all the links using current joint angles read from servo motors and forward kinematics.

To realize conforming, wheel i is pushed toward the ground while the shape of links not directly connecting to joint i is maintained [2]:

$$\begin{aligned} \dot{\theta}_{i-1}(t) &= \dot{\theta}_{i-1,w}(t) - \frac{k_a}{2} \\ \dot{\theta}_i(t) &= \dot{\theta}_{i,w}(t) + k_a \\ \dot{\theta}_{i+1}(t) &= \dot{\theta}_{i+1,w}(t) - \frac{k_a}{2} \end{aligned} \quad (4)$$

where $\dot{\theta}_{i,w}(t)$ is the increment of the angular speed for joint i produced by shape propagation in Eqn. (1) and k_a is a constant angular speed.

D. Shape propagation with active pushing

This controller pushes harder on the front side of large terrain asperities that are beneficial for propulsion while propagating a shape down the body. Different from controller C that stops pushing harder when the robot is in contact, the robot using this controller keeps pushing against asperities useful for forward propulsion after it gains contact.

To do so, we adopted an active pushing controller used on horizontal surfaces to push harder on obstacles beneficial for propulsion [13], [30]:

$$\dot{\theta}_i = \dot{\theta}_{i,w} + \sigma_i \cdot \tanh \left(\alpha \sum_{i-n_a}^{i+n_p} (\tau_i(F_i - G \cos(\phi_i))) \right) \quad (5)$$

where σ_i is the gain of the active pushing term (the second term on the right) for pitch joint i , α is a gain to tune the sensitivity of the extra bending amplitude to force/torque changes, n_a and n_p are the numbers of anterior and posterior force sensors, respectively, used for the feedback, τ_i is the torque output of pitch joint i directly read from servo motors, and G is the weight of one link added to its original form [13] to account for gravity.

Similar to controller C, an asymmetric gain σ_i [17], [30] was used in the experiments to push harder on the front side of the obstacle for larger propulsion and lighter on the back side for smaller resistance:

$$\sigma_i = \begin{cases} 3k_a, \phi_i < 0 \\ 0.1k_a, \phi_i \geq 0 \end{cases} \quad (6)$$

where k_a is a constant gain.

E. Torque-based shape propagation with head conforming to terrain

This controller was derived in [31] by optimizing bending moment to minimize the bending cost of a theoretical continuous model traversing an unknown, smooth 3-D terrain. It controls the head to conform to the terrain while the other joints follow the leader. Different from controllers A-D which control joint angles θ_i , it controls joint torque τ_i , thus inherently capable of conforming to different terrain geometry.

Here, with no real-time robot velocity information and bending in the vertical plane only, it is simplified as follows:

$$\tau_i = \begin{cases} k_\tau, i = 1 \\ K_p(\theta_i - \theta_{i-1}) + K_D \dot{\theta}_i, i \geq 2 \end{cases} \quad (7)$$

where k_τ is a constant torque to bend the head toward the ground, and K_p and K_D are constant gains. The derivative term $K_D \dot{\theta}_i$ is introduced to reduce oscillation of joints.

IV. EXPERIMENTAL SETUP & PROTOCOL

To test the performance of different controllers, we challenged the robot to traverse a half-cylindrical wooden obstacle that is 0.49 m long, 0.12 m high, and with a radius of 0.3 m, fixed onto a 2 m long wooden table (Fig. 4). The obstacle

ICRA 2022, in review

was glued together using laser-cut wooden sheets.

In all 75 trials, the robot was initially placed on the obstacle, with motor torque disabled to record initial joint angles. All wheels were contacting the terrain and the second pair of wheels were contacting both the horizontal ground and the obstacle. We started at this position instead of before the obstacle to allow robot move forward without lateral bending [8], [15]. Torque was enabled to allow controllers bend the joints after initial joint angles were recorded. A trial was ended if the robot completely traversed the obstacle, failed because of motor stalling or backward sliding out of the track, or became stuck at the same position for over one cycle of shape propagation.

To test how well the robot generated forward net propulsion, we pulled the last link of the robot with a constant horizontal backward force (similar to a drawbar test in terramechanics [32]), by hanging a weight using a string through a pulley system [21]. Weights of 200 and 400 g ($1.5\times$ and $3\times$ of the frictional drag on the flat ground [21]) were used to generate a small and large load. The weight was loaded after the torque was enabled and before the controllers started working.

To test the robot's ability to adapt to terrain variation in the front, we added another 0.16 m high, 0.32 m long obstacle in front of the half-cylindrical obstacle with a 0.26 m distance between the edges of the two obstacles (Fig. 8).

To test the robot's ability to tolerate inaccurate initial shapes with poor contact with the ground, we added a 0.23 m long, 0.1 m tall triangular wedge below the robot initially and recorded initial joint angles with the robot conforming to it under gravity while motor torque was disabled. The first pair of wheels were contacting both the horizontal ground and the wedge during this process. The wedge was then removed while the robot held its shape before controllers started working (Fig. 8F).

To track positions of the wheels, we attached an ArUco marker [33] to the side of each wheel. A high-speed camera (Adimec-N5A100-GmCXP) recorded locomotion at 100 frame/s with a resolution of 2592×2048 pixels. The camera was placed so that the obstacle was in the middle of the view to minimize lens distortion [34]. After experiments, obstacle outlines were digitized using DLTdv8 [35]. Force readings and motor angle and torque readings were recorded at 100 Hz in ROS. These data were synchronized with camera tracking data by aligning the moment when the robot started changing its shape.

To evaluate how well the robot conformed to terrain shapes, we calculated the lift-off height of all wheels in the camera view averaged spatiotemporally for each trial. Lift-off height was calculated as the vertical distance between a wheel shaft and the terrain profile offset upward by one wheel radius.

To evaluate the propulsion generated by pushing against the obstacle, we summed the horizontal components of normal forces acting on wheels contacting the obstacle. All forces were assumed to be normal to local obstacle tangent. This is inaccurate for wheels contacting both the obstacle and the ground, but its effect on results is minor because such contacts are momentary.

V. RESULTS AND DISCUSSION

Tests of backward load and terrain variations revealed nuances in how well the robot adapt to them using different controllers. Overall, position controllers with shape propagation (A-D) can generate a large propulsion given good contact. Contact force feedback controllers (B, C) helps maintain contact by adjusting bending shapes, whose performance depends on the type of sensory feedback. However, contact force feedback controllers (B, C) were challenged by extreme loads. Torque-based controller (E) inherently can conform well to terrain variation but cannot generate large propulsion without oscillations. We observed some force estimation errors from wheel pairs 2, 6, 9, and 10, which may affect the controller C and D that heavily rely on contact force feedback more than the other controllers. Below, we first briefly summarize our findings for each test, then elaborate results.

A. Traversal with no load

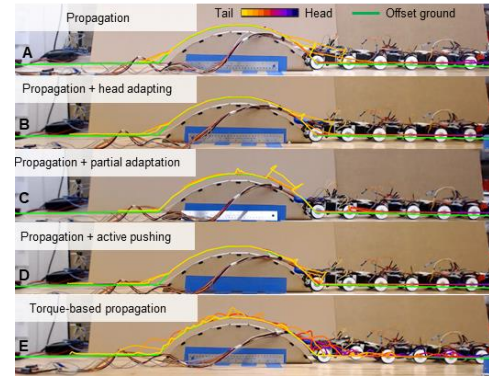


Fig. 5. Webcam snapshots of robot at the end of a representative trial with trajectories of wheel shafts overlaid for traversal with no load.

With no load, the robot traversed using all controllers (Fig. 5). Using controllers A-D, the robot showed a similar slow but steady propagation behavior (Fig. 5A-D). Traversal speed of the robot can be increased by increasing shape propagation speed and/or tuning controller gains. When propagating down the body, the initial shape conformed to the obstacle well with similar average lift-off height for controllers A-D (Fig. 10A), even for controller A with no contact force feedback. Using controller E, the robot traversed the obstacle rapidly and kept accelerating due to a lack of velocity regulation (Eqn. 7) [31]. Contact was poorer than with other controllers (Fig. 10A) because of joint oscillation (Fig. 5E).

B. Traversal with a small load

With a small additional load of $1.5\times$ frictional drag, the robot still traversed using position controllers A-D in a similar fashion as with no load (Fig. 6A-D). However, it failed to traverse using torque-based controller E (Fig. 6E).

Performance of the robot using controllers A-D was similar to that with no load (Fig. 5A-D, Fig. 10A), except that larger net propulsion was generated to overcome the larger load. Using controller E, the robot was stuck at the same position and kept oscillating up and down. This had two reasons: (1) Joint torque was insufficient to propagate the shape over the obstacle, as evidenced by decreased up and down oscillation amplitudes

of wheels near the middle of the obstacle (Fig. 4E). (2) Repetitive up and down oscillation on both sides of the obstacle produced contact forces cancelling each other. This was evidenced by the small net propulsion generated against the obstacle (Fig. 4B). We tried increasing the gain K_p to increase the torque generated. However, this resulted in larger, unstable up and down oscillation, in accordance with previous observations in propagating a pre-determined sinusoidal vertical wave in a straight slot using large gains [36].

The same gain being used for all joints made it impossible to achieve a large torque above the obstacle while stabilizing the joints elsewhere. We plan to try different gains at different joints informed by studying how force/torque distribution is related to locomotion performance.

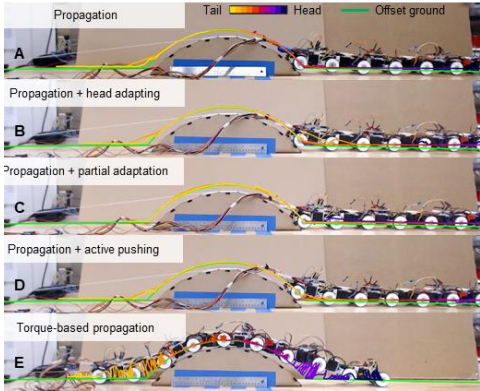


Fig. 6. Webcam snapshots of robot at the end of a representative trial with overlaid wheel shaft trajectories when robot traversed a large obstacle with a small load.

C. Traversal with a large load

With a large load of $3\times$ frictional drag, position controllers with shape propagation still generated a large propulsion if contact was well maintained. However, the large load challenged contact force feedback controllers (B and C) and resulted in loss of contact and propulsion. The torque-based controller (E) still failed to traverse similarly as with a small load.

The robot almost traversed the large obstacle with controllers A, B, and D (Fig. 7A, B, D). It generated a larger propulsion to overcome the larger load (Fig. 10B). As the robot propagated the shape down the body to achieve this, more wheels lifted off (Fig. 10A) than with a small load (Fig. 7A, B, D vs. Fig. 5 and 6). In addition, the last pair of wheels could not fully slide down the obstacle because of the large load. We plan to study how to better focus normal contact forces on surfaces with steeper orientations to further increase propulsion.

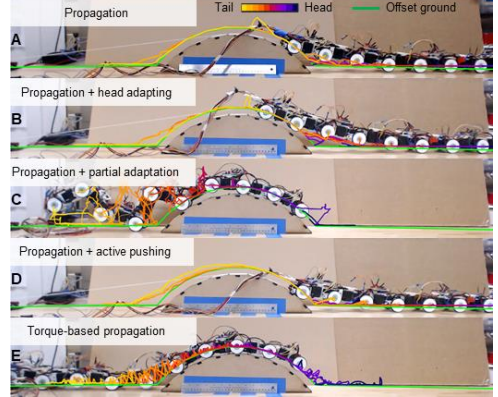


Fig. 7. Webcam snapshots of robot at the end of a representative trial with overlaid wheel shaft trajectories when robot traversed a large obstacle with large backward resistance.

The robot displayed unexpected over-bending behaviors using controller C (Fig. 7C). It started by the first pitch joint bending downward to conform to the ground after the first link was lifted up because of the large load. However, the second pitch joint did not bend to conform because it was estimated to have pitched up, resulting in an over-bending (Fig. 7C, purple trajectory detaching the terrain) that was propagated down the body (other trajectories detaching the terrain). This led to loss of contact with the front side of the obstacle and diminished forward propulsion. Eventually, the robot slid backward and failed before conforming to the terrain again. We plan to improve pitch angle estimation using an IMU and improve triggering conditions to prevent unexpected bending.

The robot using controller E still failed, likely because of insufficient torque. The robot displayed similar oscillation behaviors as with a small load (Fig. 6E) and slid backward even more under a larger backward load (Fig. 7E vs. Fig. 6E).

D. Traversal with additional obstacle in the front

The robot was able to conform to the obstacle in the front with adaptive control (controller B, C) using contact force feedback, but not otherwise (controller A, E). With feedback only used for additional pushing but not for conforming (controller D), the robot also failed.

With controllers B and C, the robot successfully traversed the entire first large obstacle and continued onto the additional obstacle until the head hit the end of the track (Fig. 8B, C). They helped the robot shape conform to the new obstacle to form new push points.

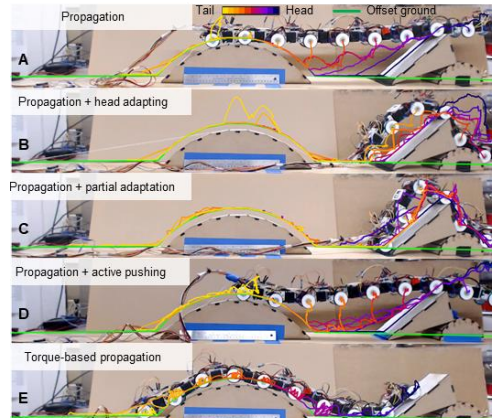


Fig. 8. Webcam snapshots of robot at the end of a representative trial with overlaid wheel shaft trajectories when robot traversed a large obstacle with another unknown obstacle in the front.

With controllers A and D, the robot climbed up the new obstacle, but could not fully detach the original large obstacle (Fig. 8A, D). Before that, the body became completely straight and the majority of the robot body lifted off the ground. This is because the controllers failed to develop new push points on the new obstacle, thus losing propulsion once the push point on the first obstacle diminished with the original bending shape. Another possible reason for failure of controller D is that the new obstacle sometimes directly contacted the robot links instead of the wheels with force sensors.

With controller E, the robot moved forward by pushing against the original obstacle and remained in contact with the ground, but it failed to ascend the additional obstacle. This was likely a result of insufficient propulsion (Fig. 10A), evidenced by similar oscillation behaviors as with a small load.

E. Traversal with poor initial terrain conformation

With poor initial terrain conformation, the robot traversed the obstacle using controllers with contact force feedback to conform to terrain geometry (B and C) or the inherently adaptive torque-based controller (F), but it failed when using controllers without contact force feedback (A) or conforming (D).

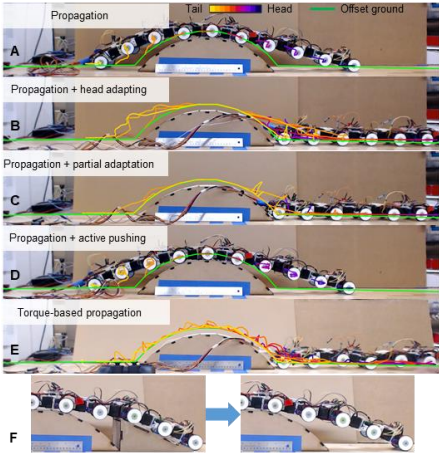


Fig. 9. (A-E) Webcam snapshot of robot at the end of a representative trial with overlaid wheel shaft trajectories when robot traversed a large obstacle with an inaccurate initial shape. (F) A wedge was placed under the robot before the robot recorded initial shape and removed before controller started working.

Using controllers B, C, and E, the robot adapted its initially inaccurate shape to one that well conformed to the terrain (Fig. 9B, C, E, Fig. 10A). With more joints involved in adaptation control using contact force feedback, controller C conformed best and generated the largest propulsion in these tests (Fig. 10).

Using controllers A and D, however, the robot simply propagated the initial shape down the robot without terrain adaptation (Fig. 9A, D). With this poorly conformed shape, the robot could not push against the front side of the obstacle (Fig. 10B) and became stuck on the obstacle.

F. Discussion

Pure shape propagation (controller A) showed consistent high performance in traversal with different loads (Figs. 4-9), indicated by the small lift-off height (Fig. 10A, white) and large

net propulsion (Fig. 10B, white). This meant that, given a shape in the vertical plane with large height variations that conforms well to the terrain, simply propagating the shape down the body will generate considerable propulsion by pushing against the height variations. However, feedforward shape propagation cannot sense and adapt to changes that cause loss of contact and push points (Fig. 8A and 9A).

Adding adaptive control to shape propagation using contact force feedback (controllers B and C) helps adapt to these changes, maintaining better contact and generating larger propulsion (Fig. 10, light and dark gray). Still, adaptation needs to be carefully applied to avoid adding resistance, as observed for controller E. For example, it should not push against the back sides of obstacles or limit contact force on points on the front side of terrain surfaces.

Shape propagation with active pushing (controller D), which works well for lateral pushing against vertical structures on flat surfaces [13], did not work well to push against terrain with large height variation using vertical bending (Fig. 8, 9E). We speculate that this is because gravity's effect on joint torques sometimes outcompetes that from contact forces. For example, additional torque is needed to hold a suspended shape.

Torque-based shape propagation with head conforming to terrain (controller E) conformed well to terrain shape changes and helped the robot traverse under a small load, but it could not generate large torque for large propulsion without introducing up and down oscillations. This is because the original controller [8] was proposed assuming no friction and did not consider the effect of gravity. Future work can add these effects to the model and derive a new control law for further testing. In addition, contact force feedback may help by varying gains for joints under different contact conditions.

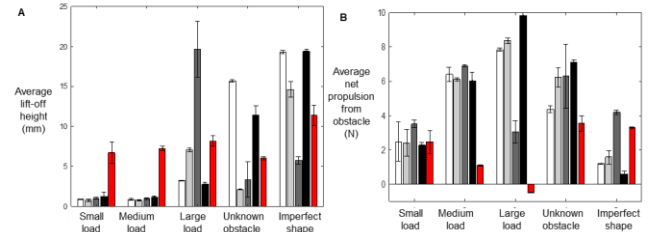


Fig. 10. Performance of different controller in different tests. (A) Lift-off height of wheels. (B) Net propulsion generated by pushing against the obstacle.

VI. SUMMARY & FUTURE WORK

By testing shape propagation controllers with different types of feedback control involved under varying load and terrain changes, we confirmed our hypotheses that: (1) Shape propagation using position control is capable of generating large propulsion by pushing against height variations, and (2) force/torque feedback is important to help adapt bending shapes to perturbation such as different loads and terrain changes, even for force control that is inherently adaptive to shape changes. This is important to for maintain contact and propulsion to traverse complex terrains.

To further improve performance in complex terrain, our current robot design needs to be improved. First, the wheels need to be replaced with larger wheels, tracks, or a smooth shell that covers a larger part of the body to prevent getting caught

ICRA 2022, in review

on terrain asperities and losing contact force information. In addition, wheels cannot handle 3-D terrains well without rolling degrees of freedom [36]. Secondly, force sensing resistors need to be better fixated to reduce errors from unknown pre-loads and occasional loss of connections. During experiments, sensors installed to wheel pairs 2, 6, 9, and 10 sometimes showed unrealistic large force readings even when the wheels were not in contact with the ground, which may affect the performance of some controllers. Using a more accurate model in calibration that considers viscoelastic behaviors of the sensors can help to improve accuracy. Considering these, our lab has developed another snake robot with contact force sensing distributed on the bottom and both sides of the body and calibrated with better models [38]. There is also much to improve in feedback controllers. For example, a combination of centralized and decentralized control [37] can save communication bandwidth for faster response speed.

ACKNOWLEDGMENT

We thank Qihan Xuan, Yifeng Zhang, Henry Astley, and Divya Ramesh for discussion.

MULTIMEDIA MATERIAL

A movie can be found at <https://youtu.be/DhPihDjTYPg>.

ICRA 2022, in review

REFERENCES

- [1] I. D. Walker, H. Choset, and G. S. Chirikjian, "Snake-like and continuum robots," in *Springer Handbook of Robotics*, vol. 4, B. Siciliano and O. Khatib, Eds. Berlin/Heidelberg, Germany: Springer, 2016, pp. 481-498.
- [2] S. Hirose, *Biologically inspired robots: snake-like locomotors and manipulators*. New York, NY: Oxford University Press, 1993.
- [3] B. C. Jayne, "Kinematics of Terrestrial Snake Locomotion," *Copeia*, vol. 1986, no. 4, pp. 915--927, 1986.
- [4] J. Gray and H. W. Lissmann, "The kinetics of the locomotion of the grass-snake," *J. Exp. Biol.*, vol. 26, no. iv, pp. 354–367, 1950.
- [5] R. M. Jorgensen and B. C. Jayne, "Three-dimensional trajectories affect the epaxial muscle activity of arboreal snakes crossing gaps," *J. Exp. Biol.*, vol. 220, no. 19, pp. 3545–3555, 2017.
- [6] P. E. Schiebel, A. M. Hubbard, and D. I. Goldman, "Comparative study of snake lateral undulation kinematics in model heterogeneous terrain," *Integr. Comp. Biol.*, p. icaa125, 2020.
- [7] T. Kano, T. Sato, R. Kobayashi, and A. Ishiguro, "Local reflexive mechanisms essential for snakes' scaffold-based locomotion," *Bioinspiration and Biomimetics*, vol. 7, no. 4, p. 046008, 2012.
- [8] H. Date and Y. Takita, "Control of 3D snake-like locomotive mechanism based on continuum modeling," in *ASME 2005 International Design Engineering Technical Conferences and Computers and Information in Engineering Conference*, 2005, pp. 1351–1359.
- [9] P. Liljeback, K. Y. Pettersen, Ø. Stavdahl, and J. T. Gravdahl, "Experimental investigation of obstacle-aided locomotion with a snake robot," *IEEE Trans. Robot.*, vol. 27, no. 4, pp. 792–800, 2011.
- [10] F. Sanfilippo, O. Stavdahl, G. Marafioti, A. A. Transeth, and P. Liljeback, "Virtual functional segmentation of snake robots for perception-driven obstacle-aided locomotion," *2016 IEEE Int. Conf. Robot. Biomimetics, ROBIO 2016*, no. 240072, pp. 1845–1851, 2016.
- [11] C. Holden, O. Stavdahl, and J. T. Gravdahl, "Optimal dynamic force mapping for obstacle-aided locomotion in 2D snake robots," in *IEEE International Conference on Intelligent Robots and Systems*, 2014, no. Iros, pp. 321–328.
- [12] T. Kamegawa, R. Kuroki, and A. Gofuku, "Evaluation of snake robot's behavior using randomized EARLI in crowded obstacles," in *12th IEEE International Symposium on Safety, Security and Rescue Robotics, SSRR 2014 - Symposium Proceedings*, 2014, pp. 1--6.
- [13] T. Kano and A. Ishiguro, "Decoding decentralized control mechanism underlying adaptive and versatile locomotion of snakes," *Integr. Comp. Biol.*, vol. 60, no. 1, pp. 232–247, 2020.
- [14] S. W. Gart, T. W. Mitchel, and C. Li, "Snakes partition their body to traverse large steps stably," *J. Exp. Biol.*, vol. 222, no. 8, p. jeb185991, 2019.
- [15] D. J. Jurestovsky, L. R. Usher, and H. C. Astley, "Generation of Propulsive Force via Vertical Undulation in Snakes," *J. Exp. Biol.*, 2021.
- [16] M. Travers, J. Whitman, and H. Choset, "Shape-based coordination in locomotion control," *Int. J. Rob. Res.*, vol. 37, no. 10, pp. 1253–1268, 2018.
- [17] T. Wang, J. Whitman, M. Travers, and H. Choset, "Directional Compliance in Obstacle-Aided Navigation for Snake Robots," in *2020 American Control Conference (ACC)*, 2020, pp. 2458–2463.
- [18] T. Takemori, M. Tanaka, and F. Matsuno, "Gait design for a snake robot by connecting curve segments and experimental demonstration," *IEEE Trans. Robot.*, vol. 34, no. 5, pp. 1384–1391, 2018.
- [19] T. Takemori, S. Member, and M. Tanaka, "Hoop-passing Motion for a Snake Robot to Realize Motion Transition across Different Environments," *IEEE Trans. Robot.*, pp. 1–16, 2020.
- [20] M. Nakajima, M. Tanaka, K. Tanaka, and F. Matsuno, "Motion control of a snake robot moving between two non-parallel planes," *Adv. Robot.*, vol. 32, no. 10, pp. 559–573, 2018.
- [21] Q. Fu and C. Li, "Robotic modeling of snake traversing large, smooth obstacles reveals stability benefits of body compliance," *R. Soc. Open Sci.*, vol. 7, no. 2, p. 191192, 2020.
- [22] Q. Fu, H. Astley, and C. Li, "How snakes traverse large obstacles in complex 3-D terrain," in *Bulletin of the American Physical Society*, 2021, vol. 66, p. P14.00012.
- [23] M. VON DURING, "Sensory nerve endings of the skin and deeper structures," *Biol. Reptil. Neurol. A*, vol. 9, pp. 407–441, 1979.
- [24] A. Crowe, "Muscle spindles, tendon organs, and joint receptors," *Sensorimotor Integr. Chicago Univ. Chicago Press*, p, pp. 454–495, 1992.
- [25] J. M. Crowe-Riddell, R. Williams, L. Chapuis, and K. L. Sanders, "Ultrastructural evidence of a mechanosensory function of scale organs (sensilla) in sea snakes (Hydrophiinae)," *R. Soc. open Sci.*, vol. 6, no. 4, p. 182022, 2019.
- [26] Q. Fu, S. W. Gart, T. W. Mitchel, J. S. Kim, G. S. Chirikjian, and C. Li, "Lateral oscillation and body compliance help snakes and snake robots stably traverse large, smooth obstacles," *Integr. Comp. Biol.*, vol. 60, no. 1, pp. 171–179, 2020.
- [27] M. Mori and S. Hirose, "Development of active cord mechanism ACM-R3 with agile 3D mobility," *Proceedings of the IEEE/RSJ International Conference on Intelligent Robots and Systems*, vol. 3, pp. 1552–1557, 2001.
- [28] P. Liljeback, Ø. Stavdahl, K. Y. Pettersen, and J. T. Gravdahl, "A modular and waterproof snake robot joint mechanism with a novel force/torque sensor," *IEEE Int. Conf. Intell. Robot. Syst.*, pp. 4898–4905, 2012.

ICRA 2022, in review

- [29] D. L. Hu, J. Nirody, T. Scott, and M. J. Shelley, “The mechanics of slithering locomotion,” *Proc. Natl. Acad. Sci.*, vol. 106, no. 25, pp. 10081–10085, 2009.
- [30] K. Yasui, N. Otaki, T. Kano, and A. Ishiguro, “Self-tunable Tegotae-based Control for Snake Locomotion,” in *2021 AMAM*, 2021.
- [31] H. Date and Y. Takita, “Adaptive locomotion of a snake like robot based on curvature derivatives,” in *IEEE International Conference on Intelligent Robots and Systems*, 2007, pp. 3554–3559.
- [32] J. Y. Wong, *Terramechanics and Off-road Vehicle Engineering: Terrain Behaviour, Off-road Vehicle Performance and Design*. Butterworth-heinemann, 2009.
- [33] S. Garrido-Jurado, R. Muñoz-Salinas, F. J. Madrid-Cuevas, and M. J. Marín-Jiménez, “Automatic generation and detection of highly reliable fiducial markers under occlusion,” *Pattern Recognit.*, vol. 47, no. 6, pp. 2280–2292, 2014.
- [34] Y. Han *et al.*, “Shape-induced obstacle attraction and repulsion during dynamic locomotion,” *Int. J. Rob. Res.*, vol. 40, no. 6–7, pp. 939–955, 2021.
- [35] T. L. Hedrick, “Software techniques for two- and three-dimensional kinematic measurements of biological and biomimetic systems,” *Bioinspiration and Biomimetics*, vol. 3, no. 3, p. 034001, 2008.
- [36] Y. Wang, T. Kamegawa, and A. Gofuku, “Study on Propulsion of a Snake Robot with Torque Propagation Based on Modified Curvature Derivatives,” in *Proceedings of 2021 IEEE International Conference on Mechatronics and Automation*, 2021, pp. 663–668.
- [37] R. Othayoth, Q. Xuan, Y. Wang, and C. Li, *Locomotor transitions in the potential energy landscape-dominated regime*, vol. 288, no. 1949, 2021.
- [38] D. Ramesh, Q. Fu, and C. Li, “SenSnake: A snake robot with contact force sensing for studying locomotion in complex 3-D terrain,” in *ICRA 2022 (submitted)*, 2022.
- [39] R. Thandiackal *et al.*, “Emergence of robust self-organized undulatory swimming based on local hydrodynamic force sensing,” *Sci. Robot.*, vol. 6, p. eabf6354, 2021.